remote sensing

MDPI

Article

Development of Spectral Disease Indices for Southern Corn Rust Detection and Severity Classification

Ran Meng [1,*,†], Zhengang Lv [1,†], Jianbing Yan [2], Gengshen Chen [2], Feng Zhao [3], Linglin Zeng [1,4] and Binyuan Xu [1]

1 College of Resources and Environment, Huazhong Agricultural University, Wuhan 430070, China; lvzhengang@webmail.hzau.edu.cn (Z.L.); zenglinglin@mail.hzau.edu.cn (L.Z.); xubinyuan@webmail.hzau.edu.cn (B.X.)
2 National Key Laboratory of Crop Genetic Improvement, Huazhong Agricultural University, Wuhan 430070, China; yjianbing@mail.hzau.edu.cn (J.Y.); gengshencgs@mail.hzau.edu.cn (G.C.)
3 College of Urban and Environmental Sciences, Central China Normal University, Wuhan 430079, China; fzhao@mail.ccnu.edu.cn
4 Guanxi Key Laboratory of Water Engineering Materials and Structures, Guanxi Institute of Water Resources Research, Nanning 530023, China
* Correspondence: mengran@mail.hzau.edu.cn; Tel.: +86-027-87282137
† These authors contributed equally to the work.

Received: 18 August 2020; Accepted: 1 October 2020; Published: 4 October 2020

Abstract: Southern Corn Rust (SCR) is one of the most destructive diseases in corn production, significantly affecting corn quality and yields globally. Field-based fast, nondestructive diagnosis of SCR is critical for smart agriculture applications to reduce pesticide use and ensure food safety. The development of spectral disease indices (SDIs), based on in situ leaf reflectance spectra, has proven to be an effective method in detecting plant diseases in the field. However, little is known about leaf spectral signatures that can assist in the accurate diagnosis of SCR, and no SDIs-based model has been reported for the field-based SCR monitoring. Here, to address those issues, we developed SDIs-based monitoring models to detect SCR-infected leaves and classify SCR damage severity. In detail, we first collected in situ leaf reflectance spectra (350–2500 nm) of healthy and infected corn plants with three severity levels (light, medium, and severe) using a portable spectrometer. Then, the RELIEF-F algorithm was performed to select the most discriminative features (wavelengths) and two band normalized differences for developing SDIs (i.e., health index and severity index) in SCR detection and severity classification, respectively. The leaf reflectance spectra, most sensitive to SCR detection and severity classification, were found in the 572 nm, 766 nm, and 1445 nm wavelength and 575 nm, 640 nm, and 1670 nm wavelength, respectively. These spectral features were associated with leaf pigment and leaf water content. Finally, by employing a support vector machine (SVM), the performances of developed SCR-SDIs were assessed and compared with 38 stress-related vegetation indices (VIs) identified in the literature. The SDIs-based models developed in this study achieved an overall accuracy of 87% and 70% in SCR detection and severity classification, 1.1% and 8.3% higher than the other best VIs-based model under study, respectively. Our results thus suggest that the SCR-SDIs is a promising tool for fast, nondestructive diagnosis of SCR in the field over large areas. To our knowledge, this study represents one of the first few efforts to provide a theoretical basis for remote sensing of SCR at field and larger scales. With the increasing use of unmanned aerial vehicles (UAVs) with hyperspectral measurement capability, more studies should be conducted to expand our developed SCR-SDIs for SCR monitoring at different study sites and growing stages in the future.

Keywords: hyperspectral measurement; change detection; vegetation stress; machine learning; smart agriculture

1. Introduction

Southern Corn Rust (SCR), caused by *Puccinia polysora* Underw, is a foliar disease, significantly affecting corn quality and yield at global scales [1,2]. In epidemic years, SCR can reduce corn production by up to 50% or even 100% [2]. Especially during recent years, the annual corn yield loss caused by SCR has increased sharply because of elevated winter minimum temperatures and the lack of SCR-resistant corn cultivars [2,3]. For example, it is estimated that in China, one of the countries most affected by SCR, the corn yield loss caused by SCR in 2015 was 756 million kg, which was as high as 8.8-times that of the annual average of 2008–2014 [2,3]. Also, in 2015, the corn yield loss caused by SCR was estimated to be 3.193 billion kg in the United States and Canada, ranking as the sixth most serious disease in terms of yield loss [4].

To control disease spread and reduce yield loss, spatial-explicit information on the disease-infected plants is indispensable in precision crop protection for guiding pesticide use and other management activities [5–7]. The development of a fast, nondestructive detection method of plant diseases (e.g., SCR) over large areas is thus a demanding challenge [6,7]. Visual inspection is the traditional method for detecting plant diseases in the field, but it is inefficient and error-prone. During recent years, remote sensing technology has shown great potential in the rapid and accurate detection of plant diseases with various crops in a nondestructive way [6,7].

Reflectance spectroscopy has been proven to be an effective approach to distinguish disease-infected leaves from healthy leaves in a fast and nondestructive way [6,8–10]. This approach utilizes changes in leaf optical properties impacted by plant disease at narrow-band wavelengths to detect plant diseases [7]. Changes in reflectance at visible wavelengths (400–700 nm) are mainly determined by pigment concentration and photosynthesis efficiency, while near-infrared (NIR, 700–1100 nm) wavelengths are strongly influenced by leaf internal structure, and shortwave infrared spectra (SWIR, 1100–2500 nm) are usually impacted by leaf water content and other biochemical compositions. Reflectance spectroscopy has been successfully applied in numerous studies for plant disease detections, such as potato late blight [8,11], rice glume blight disease [12], wheat yellow rust disease [13–15], maize dwarf mosaic and *Helminthosporium maydis* disease [16], tomato leaf diseases (e.g., late blight, target and bacterial spots) [17,18], and so on. However, the processing and analysis of reflectance spectra data with large number of narrow-band wavelengths is still complex and time-consuming [19,20].

Previous studies have indicated that some specific spectral features (wavelengths) can provide significantly higher discrimination power than others [6,7,9]. Thus, to further improve and simplify plant disease detection, researchers have developed spectral disease indices (SDIs) based on certain spectral features highly correlated to changes caused by a specific disease [9]. Using the RELIEF-F algorithm, Mahlein et al. [9] first identified the most important spectral features, and then developed SDIs most sensitive for detecting three types of leaf diseases of sugar beet (i.e., Cercospora leaf spot, sugar beet rust, and powdery mildew) based on leaf reflectance spectra. Furthermore, Bauriegel et al. [20] designed a head blight index (HBI) for detecting wheat ears infected by fusarium head blight at the early stage in the field, and results indicated that the HBI-based classification method was a promising alternative of Spectral Angle Mapper-based method using the full spectral wavelength under study, as the latter was more complicated and time-consuming. In addition, Huang et al. [21] found that photochemical reflectance index (PRI) can effectively quantify the severity of yellow rust in wheat using both in situ canopy reflectance and airborne hyperspectral measurements with a coefficient of determination (R2) of > 0.91. Similarly, Zheng et al., [22] developed optimal spectral indices for detecting yellow rust in wheat at different growth stages, based on canopy spectral reflectance measurements and the classification accuracies of all VIs-based models were above 80% in their research.

Therefore, the SDIs could potentially be a promising tool for the fast, nondestructive diagnosis of SCR in the field. However, little is known about the spectral signatures of SCR-infected leaves with different severity levels, and no SDIs-based model has been reported for detecting SCR or classifying SCR severity using in situ leaf reflectance spectra. Hence, in this study, to fill in those knowledge gaps, we proposed and evaluated SDIs-based models for detecting SCR-infected leaves and classifying their damage severity. Based on previous studies [9,23], SCR-SDIs were developed by combining single and a normalized wavelength difference from the pool of most important spectral features for the SCR monitoring. Specifically, the main objectives of this paper were to (I) characterize leaf-level spectral signatures of corn leaves infected by SCR; (II) determine the spectral features and normalized differences most important for developing SDIs in SCR detection and SCR damage severity classification, respectively; and (III) evaluate and compare the performances of our developed SCR-SDIs with the 38 stress-related vegetation indices (VIs) in the literature.

2. Materials and Methods

2.1. Study Site

The study site is in Huazhong Agricultural University Experimental Station (18.38N, 109.18E) in Sanya, Hainan province, China (Figure 1). This site is locaed in the tropical monsoon climate zone, with an average annual temperature and precipitation rate of 25.5°C and 1500 mm, respectively. Since first reported in 1972, SCR became an epidemic in Hainan annually [24]. Hainan is thus an ideal place for SCR-related studies. Based on our multiple years of planting experience, the flowering period is the critical phenological cycle for SCR monitoring in our study site. About two weeks after pollination in early January 2020, an experiment field with a natural and widespread outbreak of SCR was identified in the study site. Based on visual inspection, we did not find other major stress or disease other than the target disease, and no pesticide was applied in the experiment field. The experiment field included dozens of corn cultivars, each of which had 10 plants in total, respectively. Standard agricultural practices were conducted for the crop under study with the same water and fertilizer application throughout the growing season.

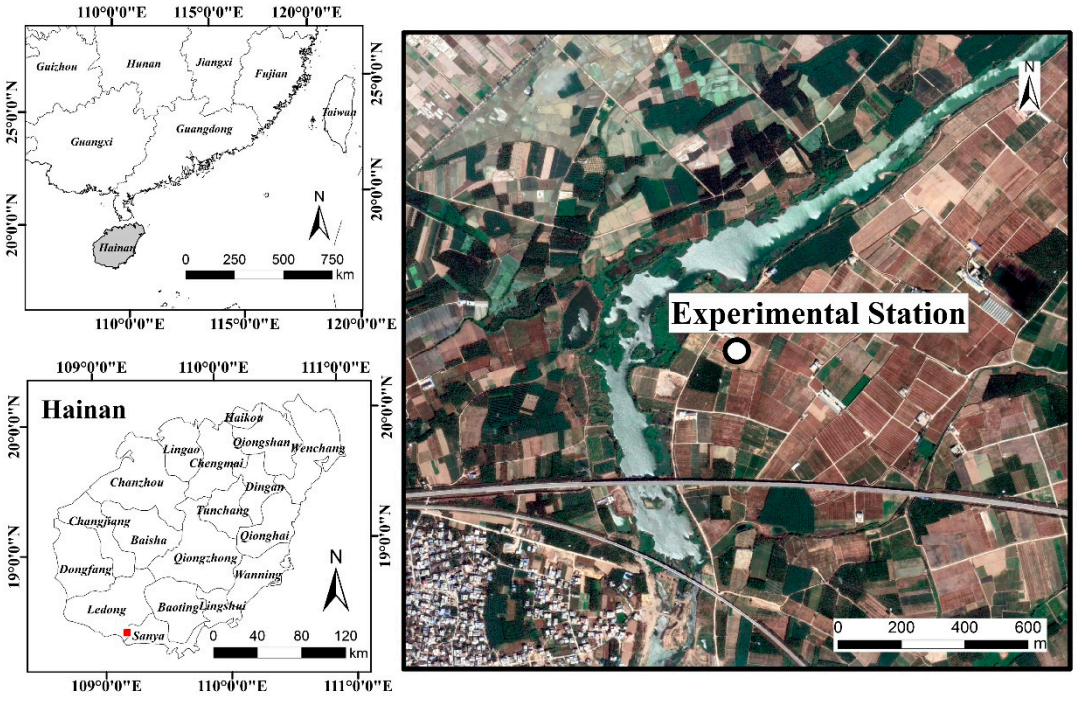

Figure 1. Location of the study site.

2.2. Methods

To monitor SCR using in situ leaf reflectance spectra, we took the following three steps (Figure 2). First, the spectra and photos of healthy and SCR-infected leaves with three levels of severity were collected in the field and pre-processed in the lab. Second, using the RELIEF-F algorithm, two SDIs for SCR detection (i.e., Healthy Index, HI) and severity classification (i.e., Severity Index, SI) were developed, respectively. Finally, based on our developed SDIs and the other 38 stress-related VIs in the literature (Table S1), different models for SCR detection and severity classification were established and compared using the Support Vector Machine (SVM) algorithm.

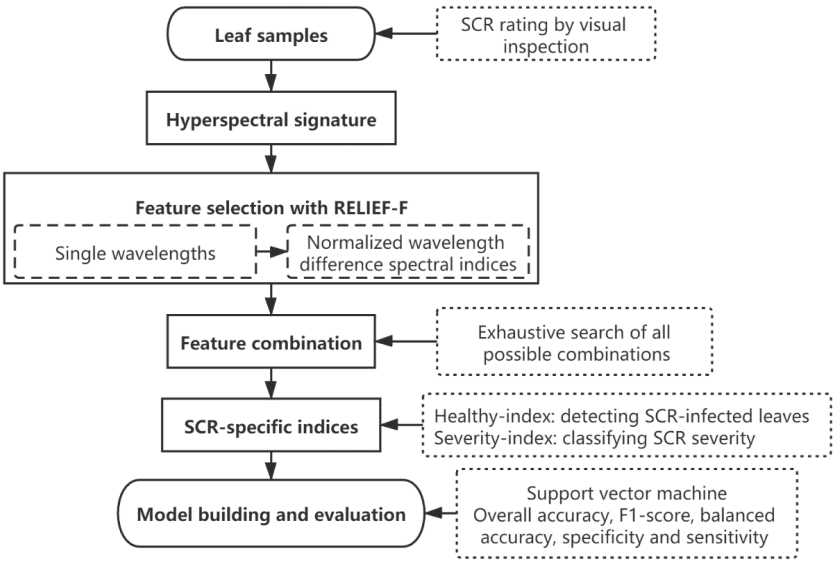

Figure 2. Flowchart of the methodology.

2.2.1. Data Acquisition and Preprocessing

We measured and recorded the healthy and SCR-infected leaves with different severity levels in the field after visual inspection. Specifically, to reduce the effects of leaf age [25,26], only the last leaf from the bottom was selected, and the selected leaves were also visually checked to make sure there was no other damage or stress than SCR. Following the procedure outlined in previous corn foliar disease studies [27,28], SCR severities were visually rated and classified into three levels based on the percentages of lesion areas on leaves by the help of a plant pathologist (Figure 3 and Table 1). Digital photographs of leaf samples were taken in the field for further reference.

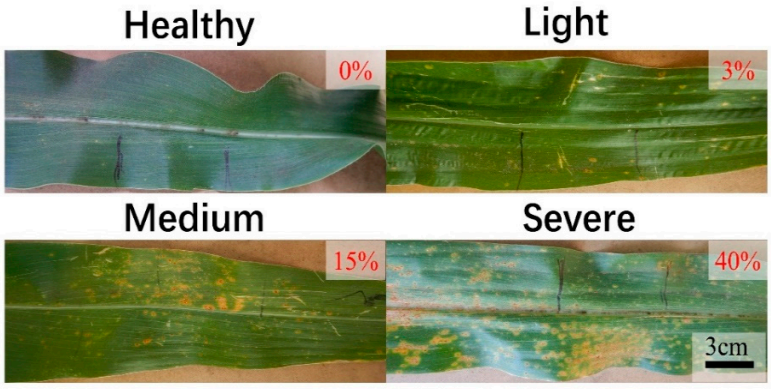

Figure 3. Healthy corn leaf and Southern Corn Rust (SCR)-infected corn leaves with different infection severities. The numbers on the upper-right side showed the visual estimations of percentage of lesion areas on leaves.

Table 1. SCR detection and severity classification scheme used in this study.

SCR Detection	SCR Severity	Percentage of Lesion Areas on Leaves	No. of Leaf Samples
Healthy	N.A.	No lesion	18
Infected	Light	<5%	16
Infected	Medium	5–29%	11
Infected	Severe	>30%	9

Finally, to reduce the potential effects of phenotype difference, 54 leaf samples from eight corn cultivars (Jing724, Jing92, Chang7-2, PH6WC, DH382, DH351, 8H534, 8H953), each of which had 6–8 leaf samples selected, of which at least one leaf sample belonged to each of three infection levels, were used for this study (Table S2).

The in situ spectral reflectance of corn leaf samples was measured using a Spectra Vista Corporation (SVC) HR-1024i spectroradiometer with a leaf clip holder attached to a pistol grip foreoptic (SVC, Poughkeepsie, NY, USA) in the daytime. The SVC spectroradiometer had a spectral range of 350–2500 nm with varied spectral resolutions (3.5 nm at 700 nm, 9.5 nm at 1500 nm, and 6.5 nm at 2100 nm). To remove the noises at the edges of spectra, only spectra between 400 nm and 2450 nm were kept and analyzed in our study. Based on a Gaussian function, the collected spectra were resampled to 1 nm for instrument output. The pistol grip foreoptic had an internal, calibrated halogen light source to illuminate the samples during leaf reflectance measurements under field conditions. For each leaf sample, reflectance spectra were measured on the upper-middle-lower parts of the leaf adaxial surface six times, and then were averaged to represent the optical properties of the whole leaf for final data analysis (Figure 3). To ensure data quality, the spectroradiometer was preheated for 20 min prior to measuring, and white reference measurements were made every 5 min using a spectralon panel (Labsphere, North Sutton, NH, USA).

2.2.2. Feature Selection and Combination

Feature selection is necessary before the development of SCR-specific SDIs, as irrelevant features (wavelengths) can increase the computation task and lead to wrong results [23,29]. There are multiple algorithms available for feature selection [25]. As the RELIEF-F algorithm is one of most classical ones and has been widely applied in the field of SDIs development, we chose it to extract the wavelengths most important for SCR detection and severity classification [9,23]. The RELIEF-F algorithm can estimate discriminative power of certain features in multiclass classification problems with incomplete and noisy data in terms of their performances in separating samples of different classes close to each other [23,30]. The RELIEF-F algorithm has been widely used in the development of SDIs for detecting plant diseases [9,23]. A weight for a feature of a measurement vector was calculated by the RELIEF-F algorithm to quantify feature relevance [23]. Generally, the RELIEF-F algorithm consists of two steps: (1) Search two nearest neighbors of the same class (hit) and from the different classes (miss) for a given number of samples in the neighborhood; (2) Calculate the weight (relevance) of each wavelength (feature) by the sum of the Euclidean distance between nearest misses and nearest hits for all samples [9,23]. Finally, wavelengths with high weight values at different spectral regions (i.e., weight values larger than 0.025-nm at 50-nm wavelength intervals) were chosen as the candidate spectral features for developing SCR-specific SDIs in our study. Before feature selection with the RELIEF-F algorithm, Savitzky–Golay smoothing was conducted to filter spectral signal noises from all samples. Savitzky–Golay smoothing and the RELIEF-F algorithm were both performed in the R environment (version 3.5.3; https://www.r-project.org/) with the packages "hsdar" and "CORElearn," respectively.

The optimized combinations of individual wavelength and a normalized wavelength difference spectral index (NDSI) (i.e., SDIs) were further selected for detecting SCR-infected leaves and classifying SCR severity, respectively [9]. In other words, we developed two SDIs according to the previous feature selection results by the RELIEF-F algorithm: The HI for discriminating healthy and SCR-infected leaves

and the SI for classifying severity of infected leaves. The formula for SDIs development is listed as follows, according to previous studies [9]:

$$SCR - specific\ indices = \frac{(a+b)}{(a-b)} + cd \quad (1)$$

where a, b, and c ($a \neq b \neq c$) are wavelengths chosen from the pool of selected wavelengths, and d is the coefficient with a value range of (−1, +1) at a step of 0.1. Here, the HI and SI were finally determined using an exhaustive search strategy [9].

2.2.3. Performances of Different Spectral Indices in SCR Detection and Severity Classification

In this study, a machine learning algorithm (i.e., SVM) was chosen to build SCR detection and severity classification model, based on the developed HI and SI, respectively. The SVM algorithm, a supervised learning method, has been widely used for detecting and classifying crop diseases [8,20]. Following previous similar studies [15,31], the radial basis function (RBF) was used as the kernel function of our SVM model for class separation, and the cost of constraints (C) and sigma (σ)—two key parameters of an SVM classifier—were determined by a grid-based search strategy [32].

A 10-fold cross validation strategy was used to evaluate and compare the performances of the developed models. Specifically, the samples were randomly split into two parts for training the SVM classifier (90%) and validating the classification accuracy (10%), respectively. This process was repeated 10 times. At last, in addition to the Overall Accuracy (OA) and Macro F1-scores of both models, the sensitivity and specificity of SCR detection model and the balanced accuracy of SCR severity model were calculated and reported (Equations (2)–(7)).

$$OA = \frac{TP + TN}{TP + FP + TN + FN} \quad (2)$$

$$F1 - score = \frac{2 * TP}{2 * TP + FP + FN} \quad (3)$$

$$Sensitivity = \frac{TP}{TP + FN} \quad (4)$$

$$Specificity = \frac{TN}{TN + FP} \quad (5)$$

$$Balanced\ accuracy = (Sensitivity + Specificity)/2 \quad (6)$$

$$Macro\ F1 - score = \frac{\sum_{i=1}^{n} (F1 - score)_i}{N} \quad (7)$$

where TP (true positive), FP (false positive), TN (true negative), and FN (false negative) are four values computed based on classification confusion matrix, and N is the number of class types under study.

In addition, the capability of SDIs in SCR detection and severity classification was compared with a total of 38 stress-related VIs in the literature (Table S1). These VIs can be grouped into three types: Simple ration indices, red edge parameters, and normalized ratio indices. Due to the large number of VIs under study, we just listed the first five most discriminative VIs in SCR detection and severity classification, respectively (Table 2). To see the whole set of implemented VIs, please refer to Table S1 in the Supplementary Materials.

Table 2. The spectral indices used for SCR detection and severity classification.

Type	Spectral Indices	Definition	Formula	Reference
Detection	D730/D706	The ratio of first derivative values at 730–706 nm	D_{730}/D_{706}	Zarco-Tejada et al. [33]
	DDI	The double difference index	$(R_{720+\Delta} - R_{720}) - (R_{672+\Delta} - R_{672})$	le Maire et al. [34]
	REP_LE	Red-edge position	$700 + 40 * ((R_{re} - R_{700})/(R_{740} - R_{700}))$	Cho and Skidmore [35]
	D715/D705	The ratio of first derivative values at 715–705 nm	D_{715}/D_{705}	Vogelmann et al. [36]
	MTCI	The MERIS Terrestrial Chlorophyll Index	$(R_{754} - R_{709}) - (R_{709} - R_{681})$	Dash and Curran [37]
Severity	DWSI	The Disease-Water stress index	R_{1660}/R_{550}	Apan et al. [38]
	PRI	The photochemical reflectance index	$(R_{531} - R_{570})/(R_{531} + R_{570})$	Gamon et al. [39]
	EGFR	The simple ratio between the maxima of the first derivatives of reflectance at the red edge and green regions	$(max(D_{650:750})/max(D_{500:550}))$	Peñuelas et al., [40]
	EGFN	The normalized ratio between the maxima of the first derivatives of reflectance at the red edge and green regions	$(max(D_{650:750}) - max(D_{500:550}))/(max(D_{650:750}) - max(D_{500:550}))$	Peñuelas et al. [40]
	SRI	Simple ratio index	R_{515}/R_{550}	Hernández-Clemente et al., [41]

This table only includes the first five most optimal spectral indices for SCR detection and severity classification, selected from 38 stress-related spectral indices in the literature. In formula, D: The first derivative of spectra; R: The base wavelengths; Δ: The integration width.

3. Results

3.1. Spectral Signatures of Healthy and SCR-Infected Corn Leaves

The mean spectra of healthy leaf and each severity group of SCR-infected leaves with standard deviation are calculated and plotted in Figure 4. In general, the leaf reflectance spectra were sensitive to SCR infection, with relatively large spectra variations at the green, red-edge, NIR, and SWIR wavelengths. Specifically, NIR reflectance, associated with leaf internal structure, decreased with severity. SWIR reflectance, associated with leaf water content and other leaf biochemical compositions, also decreased with severity. On the contrary, the reflectance at the green (550 nm) to red (680 nm) and red-edge regions (670–760 nm), most controlled by leaf chlorophyll content and photosynthesis efficiency, increased with severity.

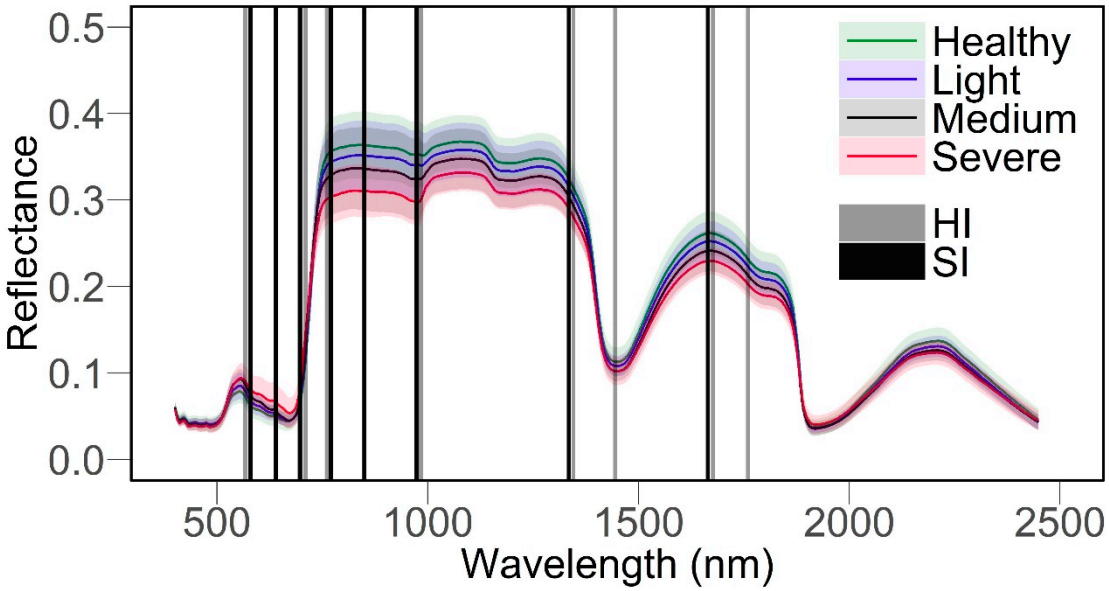

Figure 4. Mean (line) and standard deviation (shade area) of spectral reflectance of healthy and SCR-infected corn leaf groups with different severity levels. The grey and dark lines show the wavelengths selected for Health Index (HI) and Severity Index (SI) development, respectively.

3.2. SDIs for SCR Detection and Severity Classification

Based on the weight values calculated by RELIEF-F algorithm, eight discriminative wavelengths were selected to develop SDIs for detecting SCR-infected leaves (i.e., HI) and classifying SCR severity levels (i.e., SI) (Table 3 and Figure 5). There were spectral wavelengths with relatively high weight values (i.e., high discriminative power) at the green, red, red-edge, NIR and SWIR regions, consistent with our qualitative analysis on the mean spectra of healthy and SCR-infected leaves with different severity levels (Figure 4). In general, the weight values of SCR detection were mostly larger than that of SCR severity classification, but the shapes of their weight value plots were similar (Figure 5).

Table 3. Selected discriminative wavelengths for developing SCR-specific indices.

Type	Discriminative Wavelengths (nm)							
Health-index (HI)	572	707	766	980	1344	1445	1675	1760
Severity-index (SI)	575	640	702	766	850	979	1333	1670

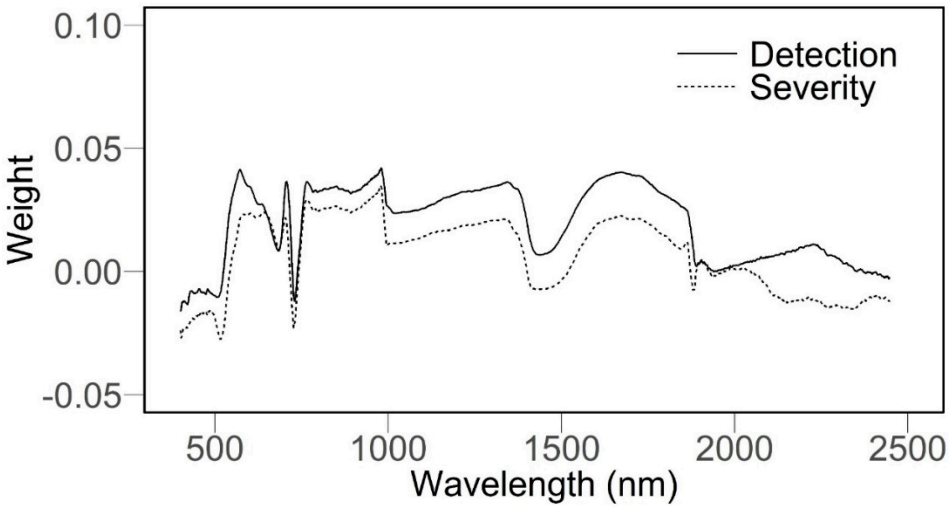

Figure 5. Wavelength weight values for SCR detection and severity classification calculated by the RELIEF-F algorithm. The higher the value, the higher the discrimination power.

Consequently, the 1445 nm, 572 nm, and 766 nm wavelengths with a coefficient value of 0.2 were selected to develop HI, and the 575 nm, 1670 nm, and 640 nm wavelengths with a coefficient value of −1 were used for developing SI (Equations (8) and (9)).

$$Health - index\ (HI) = \frac{R_{1445} - R_{572}}{R_{1445} + R_{572}} + 0.2 * R_{766} \quad (8)$$

$$Severity - index\ (SI) = \frac{R_{575} - R_{1670}}{R_{575} + R_{1670}} - R_{640} \quad (9)$$

3.3. Performances of the SCR-Specific Indices

The performance of our developed HI for detecting SCR-infected leaves was shown and compared with 38 stress-related VIs in the literature (Table S1). The validation results of the first five most discriminative VIs, among the 38 published stress-related VIs under study, are listed for detecting SCR-infected leaves in Table 4 and Figure S1 (please refer to Table S1 in the supplementary materials for the whole list). In general, the performance of HI model was the best for detecting SCR-infected leaves. The sensitivity (0.833), OA (87%), and Marco-F1 (0.856) values of the HI model were all highest among VIs under study, and the specificity value (0.889) of the HI model ranked second. The D730/D706-model also had a higher value in sensitivity (0.950), but the model specificity was much lower (0.678) compared to that of the HI model.

Table 4. Validation results of different SCR detection models using support vector machine-based 10-fold cross validation.

VIs	Specificity	Sensitivity	OA (%)	Marco-F1 Score
Heath Index (from this study)	0.833	0.889	87.0	0.856
D730/D706	0.678	0.950	85.9	0.831
DDI	0.778	0.856	83.0	0.811
REP_LE	0.711	0.828	78.9	0.766
D715/705	0.700	0.833	78.9	0.764
MTCI	0.511	0.878	75.6	0.705

Similarly, the performance of our developed SI for classifying SCR severity is shown and compared with the other VIs under study in Table 5 and Figure S2. In general, the accuracy of SCR severity

model was lower than that of SCR detection model, but the overall performance of our developed SI was still the best among VIs under study for classifying SCR severity levels. The OA (70%), Marco-F1 score (0.698), and balance accuracies of the light (0.78), medium (0.778), and severe (0.767) level were all highest.

Table 5. Validation results of the SCR severity model using the support vector machine-based 10-fold cross validation.

VIs	Balanced Accuracy			OA (%)	Marco-F1 Score
	Light	Medium	Severe		
Severity Index (from this study)	0.780	0.778	0.767	70.0	0.698
DWSI	0.769	0.708	0.637	61.7	0.589
PRI	0.775	0.489	0.778	61.7	0.526
EGFR	0.746	0.610	0.715	59.4	0.583
EGFN	0.772	0.612	0.659	59.4	0.567
SRI	0.768	0.575	0.489	54.4	0.399

4. Discussion

As stated before, the SDIs-based method for plant disease detection is computationally simple, fast, and nondestructive [9,20,23,42], which is critical for efficiently instructing the pesticide use and other management activities in crop protection in the field. This is the first study, to our knowledge, to adopt a SDIs-based (i.e., HI and SI) method for detecting SCR-infected leaves and classifying SCR damage severity. The validation results indicated that our developed SDIs outperformed 38 stress-related VIs commonly found in literature (Table S1) in terms of both SCR detection and damage severity classification (Tables 4 and 5). Our study thus highlights a fast and nondestructive method for SCR monitoring in the field compared with other techniques, like polymerase chain reaction (PCR)-based diagnostics [43,44].

4.1. Spectral Signatures of SCR-Infected Leaves

Foliar pathogens can change leaf biochemical and biophysical contents (e.g., leaf pigment, leaf water content, and leaf internal structure), and these changes can affect the leaf spectral signatures, which are the basis of the remote sensing of plant diseases [7,17,45,46]. In our study, the main influence of SCR to leaf reflectance was found in the visible (VIS) wavelength from 550 m to 700 nm, in the red-edge-NIR wavelength from 700 nm to 850 nm, and in the SWIR wavelength from 1300 nm to 1800 nm, respectively (Figures 4 and 5). The mentioned wavelengths were associated with leaf chlorophyll content, leaf water content, leaf photosynthetic efficiency, and leaf internal structure [12,22]. In addition, there were correlations between SCR damage severity and changes in VIS, red-edge, NIR, and SWIR spectral regions, making SCR severity classification possible. As the SCR severity increased, the leaf reflectance at VIS-red edge regions increased but the leaf reflectance at the NIR-SWIR regions decreased (Figures 4 and 5), which is consistent with previous studies on the remote sensing of crop disease and pests at the leaf level [9,20,23,42]. It also indicated that the SI developed here could be potentially used for quantifying the resistance of corn variety to SCR, like the phenotyping assessment of crop diseases for sugar beet and wheat [47,48].

Unlike most of the previously published similar studies on developing SDIs [9,20,23,42] which have focused on the VIS-NIR spectral range, SWIR regions were included in our study as candidate features for developing SDIs, and the feature selection results confirmed the importance of SWIR regions in both SCR detection and severity classification (Table 3 and Figure 5). Therefore, more attention should be paid to the SWIR-related VIs or features for the remote sensing of crop diseases and pests in the future. However, there is a tradeoff between performance improvement using SWIR-involved new indices and the cost increase using the equipment with SWIR measurement capability in application,

as the spectrometer with a range of 400–2500 nm is considerably more expensive than that with a range of 400–1000 nm.

We found that some of the previously published VIs (e.g., D730/D706 and DDI), sensitive to leaf chlorophyll content [33,34], had good performances in detecting SCR-infected leaves (Tables 3 and 4). When classifying severity levels for SCR damage, previously developed VIs (e.g., DWSI and PRI), sensitive to water stress [38,39], showed good results (Tables 3 and 5). This phenomenon could be explained by the fact that the SCR fungus (i.e., *Puccinia polysora* Underw) can directly generate uredium on the leaf surface, damage leaf chlorophyllous tissues, and cause leaf necrosis until the plant eventually dies [49]. In summary, it is suggested that changes in leaf chlorophyll content and leaf water content are the basis of spectral signatures of SCR.

4.2. Advantages of SDIs-Based Method for Plant Disease Monitoring

Compared to other new techniques, the SDIs-based method has several advantages that make it powerful for plant disease monitoring in the field. First, it is simple to compute. The SDIs were constructed in simple forms for easy calculations and the corresponding developed models only required light computations for implementation. In addition, no expert knowledge is required, such as the PCR-based method [7], to implement it. Second, it is fast, nondestructive, and takes only a few seconds to scan. Thus, it is possible to make repeat measurements of the same leaves and plants through their life cycle without negative effects on the crop yield, which is essential for large-scale plant disease monitoring in production. The fast screening of hundreds of plants in a short time also enables plant disease monitoring in a timely manner, which is crucial for taking appropriate measures in precision crop protection [5,50,51] and for the phenotyping of crop disease resistance in crop breeding [47,48]. Third, the SDIs-based method can make field-deployable spectra instruments for plant disease monitoring more commercially available [52,53]. A portable spectroradiometer with full-range (i.e., VIS-NIR-SWIR) measurement capability, such as the one used in this study, is expensive (~tens of thousands of US dollars), but an instrument with only certain spectra wavelengths measurement capability is much cheaper. A good example is the SPAD meter (~thousands of US dollars) for crop nitrogen estimation, which is also based on the leaf spectral measurement of certain wavelengths [54].

Our SCR detection model obtained an OA of 87% using our developed SDIs, which is comparable to previous similar studies using leaf spectral features for crop disease detection [9,13,15]. On the other hand, using the same methodology, our SCR severity model obtained an OA of 70%, which is relatively lower. The SCR detection and severity classification errors come from the fact that the reflectance standard deviations for each of the different spectral bands were relatively high and overlapped between healthy and infected leaves and among different severity classes. It is difficult to locate the bands sensitive to SCR infection and damage levels just based on visual inspection. The RELIEF-F algorithm was thus applied to locate the bands sensitive to SCR detection and severity classification, respectively (Table 3). Then, based on the selected sensitive bands, two models were developed for the rapid identification of the SCR and its severity (Tables 4 and 5). Again, the varying performances of these two kinds of model were consistent with the differences in discriminative power of spectral features (wavelengths) in SCR detection and severity classification (Figure 5). This phenomenon reflects the fact that the spectral differences between healthy and SCR-infected leaves in this study were much larger than that among SCR-infected leaves with different severity levels (Figures 4 and 5).

4.3. Limitations and Future Studies

We acknowledge that some limitations exist in this study. First, we did not evaluate our proposed method for SCR detection by considering other types of crop pest and disease, which may cause similar spectral responses of SCR. However, previous studies indicate that different crop pest and disease have their unique spectral signatures, which could be used for differentiating each other [5,9]. Second, due to the relatively small datasets, we did not evaluate the robustness and effectiveness of our developed SDIs at different maize growing stages or other study sites. However, previous similar

studies [10,19,29] in spectroscopic analysis of plant pest and disease also only used dozens of plant samples for their research. In addition, our study still serves as the one of first few efforts to explore unique spectral signatures for detecting SCR-infected leaves and classifying SCR damage severity in a rapid and nondestructive way. Thus, our study is a critical basis for remote sensing of SCR in wall-to-wall precision crop protection applications over large areas [21,55].

As an epidemic disease, SCR occurs in patches at the field scale. The fast development of unmanned aerial vehicles (UAVs) with hyperspectral capability provides an unprecedented opportunity for monitoring SCR at the field scale [56–58]. However, monitoring SCR-infected plants at the canopy level is more complicated, as the effects of canopy structure, inhomogeneous illumination conditions, leaf ages, backgrounds, and solar-view geometry to canopy spectra should be considered [25,45]. Thus, the developed SDIs-based method cannot be directly applied to UAVs-acquired hyperspectral measurements for monitoring SCR at the field scale. VI combinations (e.g., VI ratio and sum) have been shown effective to reduce the effect of the canopy structure on remote sensing of vegetation biochemical parameters [59,60]. The imaging spectroscopy technique provides a possibility to focus on disease-infected, sunny foliar areas, regardless of background materials and solar-view geometry [25,61]. More studies should thus be conducted to explore the sensitivity of various VI pairs, including our developed SDIs, to canopy structure for monitoring plant disease and pest over large areas, and a new method using imaging spectroscopy is also needed to remove the background effects in the field considering the geometry view.

Previous studies have indicated that the combined use of spectral and textural features of imaging spectroscopy can significantly improve the accuracy in crop disease detection [15]. As we used a point spectrometer for spectral reflectance measurement, only spectral features were imported as predictors in our model. Thus, the accuracies of SCR detection and severity models could likely be further improved by the combined utilization of spectral and textural features of imaging spectroscopy. In addition, considering that a hyperspectral sensor is relatively expensive, a less cost-intensive multispectral sensor mounted on UAV platform could also be potentially used for SCR monitoring over large areas, but with lower accuracies [25,52,62]. We thus recommend further studies on the developed SDIs for large-scale remote sensing of SCR at different study sites and maize growing stages with UAVs-collected imaging spectroscopy or less complex multispectral datasets [52]. Another important direction of future studies to improve disease management is the early detection of crop diseases (e.g., SCR) before the symptoms become visible [6,8,63,64]. However, due to the limited data size of this study, we did not have a chance to explore the changes in the spectral signal of SCR over time compared to the earliest SCR detection time using our proposed method. In the future, a greenhouse-based experiment, which could provide a more control environment and more samples, could be combined with field measurements to explore this direction [64,65].

5. Conclusions

In this study, we analyzed the spectral signatures of healthy and SCR-infected corn leaves and developed spectral disease indices for detecting SCR occurrences and classifying SCR damage severity. To improve efficiency and accuracy, wavelengths (features), sensitive to SCR detection (572 nm, 766 nm, and 1445 nm), and severity classification (575 nm, 640 nm, and 1670 nm), were chosen for developing SDIs (i.e., HI and SI), respectively, using the RELIEF-F algorithm, instead of the full range of spectral measurement (i.e., VIS-NIR-SWIR). The selected wavelengths concentrated on spectral regions associated with leaf chlorophyll content, leaf internal structure, and leaf water content. Finally, using SVM and SDIs, as well as 38 stress-related VIs from literature, different SCR detection and SCR severity classification models were established. A 10-fold cross-validation strategy was applied to validate and compare the performances of different models in SCR detection and severity classification. The results showed that the SDIs-based models consistently had the highest accuracies among all models, in terms of both SCR detection (OA: 87%; Marco-F1 score: 0.856) and severity classification (OA: 70%; Marco-F1 score: 0.698). Our study thus highlights a fast and nondestructive method for SCR

monitoring in the field. With the increasing use of UAVs with hyperspectral measurement capability, more studies should be conducted with our developed SDIs for remote sensing of SCR over large areas at different study sites and growing stages.

Supplementary Materials: The following are available online at http://www.mdpi.com/2072-4292/12/19/3233/s1. Table S1. 38 stress-related vegetation indices used in the study for SVM modeling; Table S2. Detailed information on leaf samples. Figure S1. Averaged confusion matrix of different SCR detection models using support vector machine based 10-fold cross validation: a. Health Index (HI); b. The ratio of first derivative values at 730–706 nm (D730/D706); c. Double Difference Index (DDI); d. The red-edge position through linear extrapolation (REP_LE); e. The ratio of first derivative values at 715–705 nm (D715/D705); f. MERIS Terrestrial Chlorophyll Index (MTCI); the fraction number in the matrix was from the 10-fold cross validation results divided by ten. Figure S2. Averaged confusion matrix of different SCR severity models using support vector machine based 10-fold cross validation: a. Severity Index (SI); b. Disease-Water Stress Index (DWSI); c. Physiological Reflectance Index (PRI); d. The simple ratio between the maxima of the first derivatives of reflectance at the red edge and green regions (EGFR); e. The normalized ratio between the maxima of the first derivatives of reflectance at the red edge and green regions (EGFN); f. Simple Ratio Index (SRI); the fraction number in the matrix was from the 10-fold cross validation results divided by ten. R source codes for SVM-based SCR detection and severity classification modeling; SCR samples in csv format.

Author Contributions: Conceptualization, R.M.; methodology, R.M., Z.L., and G.C.; formal analysis, R.M., Z.L., G.C., and B.X.; resources, R.M. and J.Y.; writing—original draft preparation R.M. and Z.L.; writing—review and editing, R.M., Z.L., J.Y., G.C., F.Z., L.Z., and B.X.; funding acquisition, R.M. All authors have read and agreed to the published version of the manuscript.

Funding: This work was supported by the Fundamental Research Funds for the Central Universities (No.2662019PY057).

Acknowledgments: The authors would like to thank the Fundamental Research Funds for the Central Universities (No.2662019PY057). We also would like to thank the help and hard work of four anonymous reviewers and journal editors.

Conflicts of Interest: The authors declare that they have no known competing financial interests or personal relationships that could have appeared to influence the work reported in this manuscript.

References

1. Brewbaker, J.L.; Kim, S.K.; So, Y.S.; Logroño, M.; Moon, H.G.; Ming, R.; Lu, X.W.; Josue, A.D. General Resistance in Maize to Southern Rust (Puccinia polysora Underw.). *Crop Sci.* **2011**, *51*, 1393–1409. [CrossRef]
2. Liu, J.; Jiang, Y.; Zeng, J.; Ji, G.; Liu, L.; Qiu, K.; Xu, Y. Analysis of the main occurrence characteristics and causes of the southern corn rust in China in 2015. *China Plant Prot.* **2016**, *36*, 44–47.
3. Liu, J.; Ma, Q.; Yu, K.; Wang, X. A report about the occurrence area of southern corn rust and the resistance of the corn cultivars in china. *Crops* **2009**, *3*, 71–75.
4. Mueller, D.; Wise, K.; Sisson, A.; Allen, T.; Bergstrom, G.; Bosley, D.; Bradley, C.; Broders, K.; Byamukama, E.; Chilvers, M.; et al. Corn Yield Loss Estimates Due to Diseases in the United States and Ontario, Canada from 2012 to 2015. *Plant Health Prog.* **2016**, *17*, 211–222. [CrossRef]
5. Mahlein, A.K.; Oerke, E.-C.; Steiner, U.; Dehne, H.-W. Recent advances in sensing plant diseases for precision crop protection. *Eur. J. Plant Pathol.* **2012**, *133*, 197–209. [CrossRef]
6. Mahlein, A.K.; Kuska, M.T.; Behmann, J.; Polder, G.; Walter, A. Hyperspectral Sensors and Imaging Technologies in Phytopathology: State of the Art. *Annu. Rev. Phytopathol.* **2018**, *56*, 535–558. [CrossRef]
7. Zhang, J.; Huang, Y.; Pu, R.; Gonzalez-Moreno, P.; Yuan, L.; Wu, K.; Huang, W. Monitoring plant diseases and pests through remote sensing technology: A review. *Comput. Electron. Agric.* **2019**, *165*, 104943. [CrossRef]
8. Gold, K.M.; Townsend, P.A.; Chlus, A.; Herrmann, I.; Couture, J.J.; Larson, E.R.; Gevens, A.J. Hyperspectral measurements enable pre-symptomatic detection and differentiation of contrasting physiological effects of late blight and earrly blight in potato. *Remote Sens.* **2020**, *12*, 286. [CrossRef]
9. Mahlein, A.K.; Rumpf, T.; Welke, P.; Dehne, H.W.; Plumer, L.; Steiner, U.; Oerke, E.C. Development of spectral indices for detecting and identifying plant diseases. *Remote Sens. Environ.* **2013**, *128*, 21–30. [CrossRef]
10. Naidu, R.A.; Perry, E.M.; Pierce, F.J.; Mekuria, T. The potential of spectral reflectance technique for the detection of Grapevine leafroll-associated virus-3 in two red-berried wine grape cultivars. *Comput. Electron. Agric.* **2009**, *66*, 38–45. [CrossRef]

11. Gold, K.M.; Townsend, P.A.; Herrmann, I.; Gevens, A.J. Investigating potato late blight physiological differences across potato cultivars with spectroscopy and machine learning. *Plant Sci.* **2019**. [CrossRef] [PubMed]
12. Liu, Z.Y.; Wu, H.F.; Huang, J.F. Application of neural networks to discriminate fungal infection levels in rice panicles using hyperspectral reflectance and principal components analysis. *Comput. Electron. Agric.* **2010**, *72*, 99–106. [CrossRef]
13. Zhang, J.; Pu, R.; Huang, W.; Yuan, L.; Luo, J.; Wang, J. Using in-situ hyperspectral data for detecting and discriminating yellow rust disease from nutrient stresses. *Field Crops Res.* **2012**, *134*, 165–174. [CrossRef]
14. Bravo, C.; Moshou, D.; West, J.; McCartney, A.; Ramon, H. Early disease detection in wheat fields using spectral reflectance. *Biosyst. Eng.* **2003**, *84*, 137–145. [CrossRef]
15. Guo, A.; Huang, W.; Ye, H.; Dong, Y.; Ma, H.; Ren, Y.; Ruan, C. Identification of Wheat Yellow Rust using Spectral and Texture Features of Hyperspectral Images. *Remote Sens.* **2020**, *12*, 1419. [CrossRef]
16. Ausmus, B.S.; Hilty, J.W. Reflectance studies of healthy, maize dwarf mosaic virus-infected, and Helminthosporium maydis-infected corn leaves. *Remote Sens. Environ.* **1971**, *2*, 77–81. [CrossRef]
17. Jones, C.D.; Jones, J.B.; Lee, W.S. Diagnosis of bacterial spot of tomato using spectral signatures. *Comput. Electron. Agric.* **2010**, *74*, 329–335. [CrossRef]
18. Lu, J.Z.; Ehsani, R.; Shi, Y.Y.; de Castro, A.I.; Wang, S. Detection of multi-tomato leaf diseases (late blight, target and bacterial spots) in different stages by using a spectral-based sensor. *Sci. Rep.* **2018**, *8*, 2793. [CrossRef]
19. Chen, T.; Zeng, R.; Guo, W.; Hou, X.; Lan, Y.; Zhang, L. Detection of Stress in Cotton (Gossypium hirsutum L.) Caused by Aphids Using Leaf Level Hyperspectral Measurements. *Sensors* **2018**, *18*, 2798. [CrossRef]
20. Bauriegel, E.; Giebel, A.; Geyer, M.; Schmidt, U.; Herppich, W.B. Early detection of Fusarium infection in wheat using hyper-spectral imaging. *Comput. Electron. Agric.* **2011**, *75*, 304–312. [CrossRef]
21. Huang, W.; Lamb, D.W.; Niu, Z.; Zhang, Y.; Liu, L.; Wang, J. Identification of yellow rust in wheat using in-situ spectral reflectance measurements and airborne hyperspectral imaging. *Precis. Agric.* **2007**, *8*, 187–197. [CrossRef]
22. Zheng, Q.; Huang, W.; Cui, X.; Dong, Y.; Shi, Y.; Ma, H.; Liu, L. Identification of Wheat Yellow Rust Using Optimal Three-Band Spectral Indices in Different Growth Stages. *Sensors* **2018**, *19*, 35. [CrossRef] [PubMed]
23. Shirzadifar, A.; Bajwa, S.; Nowatzki, J.; Shojaeiarani, J. Development of spectral indices for identifying glyphosate-resistant weeds. *Comput. Electron. Agric.* **2020**, *170*, 105276. [CrossRef]
24. Mu, C.; Lu, S.; Fu, J.; Zhang, F.; Li, W.; Sun, Q.; Zhang, X.; Meng, Z. Research Progress on Southern Corn Rust. *Fujian J. Agric. Sci.* **2013**, *25*, 509–512.
25. Bohnenkamp, D.; Behmann, J.; Mahlein, A.K. In-Field detection of yellow rust in wheat on the ground canopy and UAV scale. *Remote Sens.* **2019**, *11*, 2495. [CrossRef]
26. Wu, J.; Rogers, A.; Albert Loren, P.; Ely, K.; Prohaska, N.; Wolfe Brett, T.; Oliveira Raimundo, C.; Saleska Scott, R.; Serbin Shawn, P. Leaf reflectance spectroscopy captures variation in carboxylation capacity across species, canopy environment and leaf age in lowland moist tropical forests. *New Phytol.* **2019**, *224*, 663–674. [CrossRef] [PubMed]
27. Zhao, P.; Zhang, G.; Wu, X.; Li, N.; Shi, D.; Zhang, D.; Ji, C.; Xu, M.; Wang, S. Fine mapping of RppP25, a southern rust resistance gene in maize. *J. Integr. Plant Biol.* **2013**, *55*, 462–472. [CrossRef] [PubMed]
28. Kump, K.L.; Bradbury, P.J.; Wisser, R.J.; Buckler, E.S.; Belcher, A.R.; Oropeza-Rosas, M.A.; Zwonitzer, J.C.; Kresovich, S.; McMullen, M.D.; Ware, D.; et al. Genome-wide association study of quantitative resistance to southern leaf blight in the maize nested association mapping population. *Nat. Genet.* **2011**, *43*, 163–168. [CrossRef]
29. Meng, R.; Dennison, P.E. Spectroscopic analysis of green, desiccated and dead tamarisk canopies. *Photogramm. Eng. Remote Sens.* **2015**, *81*, 199–207.
30. Robnik-Sikonja, M.; Kononenko, I. Theoretical and empirical analysis of ReliefF and RReliefF. *Mach. Learn.* **2003**, *53*, 23–69. [CrossRef]
31. Amari, S.; Wu, S. Improving support vector machine classifiers by modifying kernel functions. *Neural Netw.* **1999**, *12*, 783–789. [CrossRef]
32. Hsu, C.-W.; Chang, C.-C.; Lin, C.-J. *A Practical Guide to Support Vector Classification*; National Taiwan University: Taipei, Taiwan, 2003.

33. Zarco-Tejada, P.J.; Pushnik, J.C.; Dobrowski, S.; Ustin, S.L. Steady-state chlorophyll a fluorescence detection from canopy derivative reflectance and double-peak red-edge effects. *Remote Sens. Environ.* **2003**, *84*, 283–294. [CrossRef]
34. le Maire, G.; François, C.; Dufrêne, E. Towards universal broad leaf chlorophyll indices using PROSPECT simulated database and hyperspectral reflectance measurements. *Remote Sens. Environ.* **2004**, *89*, 1–28. [CrossRef]
35. Cho, M.A.; Skidmore, A.K. A new technique for extracting the red edge position from hyperspectral data: The linear extrapolation method. *Remote Sens. Environ.* **2006**, *101*, 181–193. [CrossRef]
36. Vogelmann, J.E.; Rock, B.N.; Moss, D.M. Red edge spectral measurements from sugar maple leaves. *Int. J. Remote Sens.* **1993**, *14*, 1563–1575. [CrossRef]
37. Dash, J.; Curran, P.J. The MERIS terrestrial chlorophyll index. *Int. J. Remote Sens.* **2004**, *25*, 5403–5413. [CrossRef]
38. Apan, A.; Held, A.; Phinn, S.; Markley, J. Detecting sugarcane 'orange rust' disease using EO-1 Hyperion hyperspectral imagery. *Int. J. Remote Sens.* **2004**, *25*, 489–498. [CrossRef]
39. Gamon, J.A.; Penuelas, J.; Field, C.B. A narrow-waveband spectral index that tracks diurnal changes in photosynthetic efficiency. *Remote Sens. Environ.* **1992**, *41*, 35–44. [CrossRef]
40. Peñuelas, J.; Gamon, J.A.; Fredeen, A.L.; Merino, J.; Field, C.B. Reflectance indices associated with physiological changes in nitrogen- and water-limited sunflower leaves. *Remote Sens. Environ.* **1994**, *48*, 135–146. [CrossRef]
41. Hernández-Clemente, R.; Navarro-Cerrillo, R.M.; Zarco-Tejada, P.J. Carotenoid content estimation in a heterogeneous conifer forest using narrow-band indices and PROSPECT+DART simulations. *Remote Sens. Environ.* **2012**, *127*, 298–315. [CrossRef]
42. Zheng, Q.; Huang, W.; Cui, X.; Shi, Y.; Liu, L. New Spectral Index for Detecting Wheat Yellow Rust Using Sentinel-2 Multispectral Imagery. *Sensors* **2018**, *18*, 868. [CrossRef] [PubMed]
43. Crouch, J.A.; Szabo, L.J. Real-Time PCR Detection and Discrimination of the Southern and Common Corn Rust Pathogens Puccinia polysora and Puccinia sorghi. *Plant Dis.* **2011**, *95*, 624–632. [CrossRef] [PubMed]
44. Sankaran, S.; Mishra, A.; Ehsani, R.; Davis, C. A review of advanced techniques for detecting plant diseases. *Comput. Electron. Agric.* **2010**, *72*, 1–13. [CrossRef]
45. Lopez-Lopez, M.; Calderon, R.; Gonzalez-Dugo, V.; Zarco-Tejada, P.J.; Fereres, E. Early Detection and Quantification of Almond Red Leaf Blotch Using High-Resolution Hyperspectral and Thermal Imagery. *Remote Sens.* **2016**, *8*, 276. [CrossRef]
46. Adam, E.; Deng, H.; Odindi, J.; Abdel-Rahman, E.M.; Mutanga, O. Detecting the Early Stage of Phaeosphaeria Leaf Spot Infestations in Maize CroUsing in Situ Hyperspectral Data and Guided Regularized Random Forest Algorithm. *J. Spectrosc.* **2017**, *2017*, 6961387. [CrossRef]
47. Leucker, M.; Wahabzada, M.; Kersting, K.; Peter, M.; Beyer, W.; Steiner, U.; Mahlein, A.K.; Oerke, E.C. Hyperspectral imaging reveals the effect of sugar beet quantitative trait loci on Cercospora leaf spot resistance. *Funct. Plant Biol.* **2017**, *44*, 1–9. [CrossRef]
48. Alisaac, E.; Behmann, J.; Kuska, M.T.; Dehne, H.W.; Mahlein, A.K. Hyperspectral quantification of wheat resistance to Fusarium head blight: Comparison of two Fusarium species. *Eur. J. Plant Pathol.* **2018**, *152*, 869–884. [CrossRef]
49. Wanlayaporn, K.; Authrapun, J.; Vanavichit, A.; Tragoonrung, S. QTL Mapping for Partial Resistance to Southern Corn Rust Using RILs of Tropical Sweet Corn. *Am. J. Plant Sci.* **2013**, *4*, 878–889. [CrossRef]
50. Bohnenkamp, D.; Kuska, M.T.; Mahlein, A.K.; Behmann, J. Hyperspectral signal decomposition and symptom detection of wheat rust disease at the leaf scale using pure fungal spore spectra as reference. *Plant Pathol.* **2019**, *68*, 1188–1195. [CrossRef]
51. Kuska, M.T.; Behmann, J.; Namini, M.; Oerke, E.C.; Steiner, U.; Mahlein, A.K. Discovering coherency of specific gene expression and optical reflectance properties of barley genotypes differing for resistance reactions against powdery mildew. *PLoS ONE* **2019**, *14*, e0213291. [CrossRef]
52. Kuska, M.T.; Behmann, J.; Grosskinsky, D.K.; Roitsch, T.; Mahlein, A.K. Screening of Barley Resistance Against Powdery Mildew by Simultaneous High-Throughput Enzyme Activity Signature Profiling and Multispectral Imaging. *Front. Plant Sci.* **2018**, *9*, 1074. [CrossRef] [PubMed]

53. Thomas, S.; Kuska, M.T.; Bohnenkamp, D.; Brugger, A.; Alisaac, E.; Wahabzada, M.; Behmann, J.; Mahlein, A.K. Benefits of hyperspectral imaging for plant disease detection and plant protection: A technical perspective. *J. Plant Dis. Prot.* **2018**, *125*, 5–20. [CrossRef]
54. Yang, H.; Yang, J.P.; Lv, Y.M.; He, J.J. SPAD Values and Nitrogen Nutrition Index for the Evaluation of Rice Nitrogen Status. *Plant Prod. Sci.* **2014**, *17*, 81–92. [CrossRef]
55. Zhang, D.; Zhou, X.; Zhang, J.; Lan, Y.; Xu, C.; Liang, D. Detection of rice sheath blight using an unmanned aerial system with high-resolution color and multispectral imaging. *PLoS ONE* **2018**, *13*, e0187470. [CrossRef]
56. Sankey, T.; Donager, J.; McVay, J.; Sankey, J.B. UAV lidar and hyperspectral fusion for forest monitoring in the southwestern USA. *Remote Sens. Environ.* **2017**, *195*, 30–43. [CrossRef]
57. Zhang, X.; Han, L.; Dong, Y.; Shi, Y.; Huang, W.; Han, L.; González-Moreno, P.; Ma, H.; Ye, H.; Sobeih, T. A Deep Learning-Based Approach for Automated Yellow Rust Disease Detection from High.-Resolution Hyperspectral UAV Images. *Remote Sens.* **2019**, *11*, 1554. [CrossRef]
58. Meng, R.; Yang, D.; McMahon, A.; Hantson, W.; Hayes, D.; Breen, A.; Serbin, S. A UAS Platform for Assessing Spectral, Structural, and Thermal Patterns of Arctic Tundra Vegetation. In Proceedings of the IGARSS 2019–2019 IEEE International Geoscience and Remote Sensing Symposium, Yokohama, Japan, 28 July–2 August 2019.
59. Xu, M.Z.; Liu, R.G.; Chen, J.M.; Liu, Y.; Shang, R.; Ju, W.M.; Wu, C.Y.; Huang, W.J. Retrieving leaf chlorophyll content using a matrix-based vegetation index combination approach. *Remote Sens. Environ.* **2019**, *224*, 60–73. [CrossRef]
60. Haboudane, D.; Tremblay, N.; Miller, J.R.; Vigneault, P. Remote estimation of crop chlorophyll content using spectral indices derived from hyperspectral data. *IEEE Trans. Geosci. Remote Sens.* **2008**, *46*, 423–437. [CrossRef]
61. Ali, M.M.; Bachik, N.A.; Muhadi, N.A.; Yusof, T.N.T.; Gomes, C. Non-destructive techniques of detecting plant diseases: A review. *Physiol. Mol. Plant Pathol.* **2019**, *108*, 101426. [CrossRef]
62. Tane, Z.; Roberts, D.; Koltunov, A.; Sweeney, S.; Ramirez, C. A framework for detecting conifer mortality across an ecoregion using high spatial resolution spaceborne imaging spectroscopy. *Remote Sens. Environ.* **2018**, *209*, 195–210. [CrossRef]
63. Rumpf, T.; Mahlein, A.K.; Steiner, U.; Oerke, E.C.; Dehne, H.W.; Plümer, L. Early detection and classification of plant diseases with Support. Vector Machines based on hyperspectral reflectance. *Comput. Electron. Agric.* **2010**, *74*, 91–99. [CrossRef]
64. Mahlein, A.K.; Alisaac, E.; Al Masri, A.; Behmann, J.; Dehne, H.W.; Oerke, E.C. Comparison and combination of thermal, fluorescence, and hyperspectral imaging for monitoring fusarium head blight of wheat on spikelet scale. *Sensors* **2019**, *19*, 2281. [CrossRef] [PubMed]
65. Mahlein, A.K.; Kuska, M.T.; Thomas, S.; Wahabzada, M.; Behmann, J.; Rascher, U.; Kersting, K. Quantitative and qualitative phenotyping of disease resistance of crops by hyperspectral sensors: Seamless interlocking of phytopathology, sensors, and machine learning is needed! *Curr. Opin. Plant Biol.* **2019**, *50*, 156–162. [CrossRef] [PubMed]